Post-print version:

Distributed frequency control with partial information using MT-HVDC grids and WPPs

F.D. Bianchi, J.L. Domínguez-García and T. Vrana

This work has been published in **IEEE Systems Journal**:

F.D. Bianchi, J.L. Domínguez-García and T. Vrana, "Distributed frequency control with partial information using MT-HVDC grids and WPPs", *IEEE Systems Journal*, vol. 13, no. 2, pp. 1694-1701, 2019.

Final version available at:

URL: https://ieeexplore.ieee.org/document/8470249

DOI: 10.1109/JSYST.2018.2869547

BibTex:

```
@Article{Bianchi2016,
    Title    = {Distributed frequency control with partial information using MT-HVDC
       grids and WPPs},
    Author   = {Fernando D. Bianchi and José Luis Domínguez-García and Til Kristian
       Vrana},
    Journal  = {IEEE Systems Journal},
    Year     = {2019},
    Number   = {2},
    Pages    = {1694-1701},
    Volume   = {13},
    Doi      = {10.1109/JSYST.2018.2869547}
}
```

Distributed frequency control with partial information using MT-HVDC grids and WPPs

Fernando D. Bianchi, *Member IEEE*, José Luis Domínguez-García, and Til Kristian Vrana

***Abstract*—Expansion of offshore wind power and the use of HVDC technologies in power transmission are modifying the power system dynamics making them more sensitive to power disturbances. Thus, in order to ensure power system secure and stable operation, transmission system operators are requiring wind power and HVDC systems to provide ancillary services such as frequency support. In this paper, a distributed control scheme is proposed to coordinate the contribution of wind power plants (WPPs) to mitigate frequency deviations in isolated AC synchronous areas connected through a multi-terminal HVDC grid. The control scheme aims to share the power reserves with limited information exchange.**

***Index Terms*—Distributed control, primary frequency support, reduced information, grid integration, multi–terminal HVDC grids, wind power plants**

I. Introduction

OFFSHORE wind power installations have being rapidly growing in the last years mainly due to limitations in onshore locations but also due to better wind conditions that can be found far from shore [1]. The trend in the new offshore wind power plants (WPPs) is towards larger power ratings and longer distances between generation and inland consumptions. For this scenario, the most suitable power transmission technology is based on High Voltage Direct Current (HVDC). The increase of offshore WPPs and the need for additional cross-border electrical interconnections is also fostering the view of wind farms as electrical offshore nodes [2], and the use of an additional meshed power transmission grid based on Multi-terminal HVDC (MT-HVDC) technology [3]. This kind of networks may also provide higher power flow controllability through the different terminals [4], [5].

The power system frequency is the active power balance indicator in an AC grid, giving frequency control a high priority. The frequency has to be kept in a narrow operation range for a variety of reasons. The system inertia is crucial for dynamic frequency stability, since it covers short-term imbalances (seconds range) and limits the rate of change of frequency [6]. This important system inertia is subject to an ongoing continuous reduction. The system inertia is based on the inertia of all directly grid-connected rotating three-phase electrical machines. Exactly these essential sources of system inertia are slowly disappearing, as more and more of these directly connected machines are replaced with other machines with power-converter interfaces as wind power generation and HVDC technologies [7].

Primary frequency control is traditionally provided by conventional power stations, and every synchronous area has its own generation reserves for primary frequency control [8]. With the trend towards sustainable power sources, the share of synchronous-machine-based conventional power stations is decreasing. This leads Transmission System Operators (TSOs) to require both any generation technology and HVDC based systems to provide support to ensure frequency stability [7]. Thus, power electronic based technologies may provide such support through the regulation of active power injection [5], [9].

Wind power can only use two approaches to provide frequency support: releasing part of the kinetic energy stored in the wind rotors (slowing down the wind turbine) or temporally increasing the power production, for which it is necessary to keep certain generation capacity reserve (see e.g. [10]–[12]). From MT-HVDC system side, frequency control may be achieved through sharing of reserves between synchronous areas (see e.g. [13]–[16]). Recently, some authors have proposed the provision of frequency support using WPPs connected through MT-HVDC grids [17]–[20].

This paper introduces a distributed control scheme aimed to coordinate the power contributions of WPPs and AC areas connected through a MT-HVDC grids. The purpose is to share power reserves and thus minimize frequency deviations in AC areas. This work extends the results in [20] considering MT-HVDC systems with less communication links, local power control in AC areas, which allows to restore the wind power reserves, and droop control for DC voltage regulation, which is a well-accepted strategy for ensuring the power transmission. In addition, the new control requires less information exchange among agents, simplifying the implementation and improving reliability.

II. MT-HVDC networks with WPPs and AC areas

Figure 1 sketches the system under study consisted of a MT-HVDC grid, n AC areas and m WPPs. Voltage Source Converters (VSCs) are used to connect the AC areas and WPPs to the DC grid. The main purpose of the MT-HVDC network is the power transmission from the WPPs to the consumptions in the AC areas. In addition, the system may also help in the primary frequency control in the AC areas. This implies that

F.D. Bianchi is with Instituto Balseiro and CONICET, Av. Bustillo 9500, S.C. Bariloche, Argentina. e-mail: fernando.bianchi@ib.edu.ar

J.L. Domínguez-García is with Catalonia Institute for Energy Research, IREC, Jardins de les Dones de Negre 1, 08930 Sant Adrià de Besòs, Barcelona, Spain.

T.K. Vrana is with SINTEF Energi, Trondheim, Norway.

This work was partially supported by the EU 7th framework programs FP7-ENERGY-2013 IRPWIND Project (under Grant Agreement 609795). The work of F.Bianchi and J.L. Domínguez-García was also supported by the CERCA Programme from the Generalitat de Catalunya.

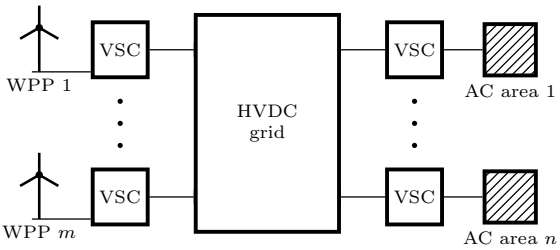

Figure 1. Schematic representation of a MT-HVDC network connecting AC areas and WPPs [20]

WPPs must be capable of increasing the active power delivered to the grid in order to temporally balance consumption and generation in the AC areas and thus limit the frequency deviations. This power available for provision of ancillary services is commonly known as power reserve.

A. AC area modelling

Commonly for frequency control studies, AC areas are modelled as a single aggregated synchronous generator with a load depending on the frequency [8]. This is a reasonable approximation as the response of AC grids based on conventional power sources is dominated by slow synchronous generators. Therefore, the dynamics of the j-th AC area ($j = 1, \dots, n$) can be expressed by

$$\frac{\mathrm{d}f_j}{\mathrm{d}t} = \frac{P_{g,j} - P_{l,j} - P_{\mathrm{dc},j}}{4\pi^2 \bar{f}_j J_j} - \left(\frac{P_{l,j} D_{l,j}}{4\pi^2 \bar{f}_j J_j} + \frac{D_{g,j}}{J_j}\right)(f_j - \bar{f}_j), \quad (1)$$

$$\frac{\mathrm{d}P_{g,j}}{\mathrm{d}t} = \frac{1}{\tau_{g,j}}(P_{r,j} - P_{g,j}), \quad (2)$$

where f_j is the electrical frequency, $\bar{f}_j$ is the nominal frequency, J_j and $D_{g,j}$ are the inertia and the generator damping, respectively, $D_{l,j}$ is the load damping, $P_{g,j}$ is the mechanical power, $P_{l,j}$ is the power demand in the area, and $P_{\mathrm{dc},j}$ is the DC power extracted from the multi-terminal network. Equation (2) corresponds to the speed governor in the synchronous generator, where $\tau_{g,j}$ is the time constant and $P_{r,j}$ is the set-point.

Linearizing (1) and using the following incremental variables

$$y_j = f_j - \bar{f}_j, \qquad x_j = P_{g,j} - \bar{P}_{g,j},$$
$$u_j = P_{\mathrm{dc},j} - \bar{P}_{\mathrm{dc},j}, \qquad d_j = P_{l,j} - \bar{P}_{l,j},$$
$$q_j = P_{r,j} - \bar{P}_{r,j},$$

the small-signal dynamics of the j-th AC area is given by

$$\frac{\mathrm{d}y_j}{\mathrm{d}t} = -a_{1,j} y_j + a_{2,j}(x_j - d_j - u_j), \quad (3)$$

$$\frac{\mathrm{d}x_j}{\mathrm{d}t} = -a_{3,j} x_j + a_{3,j} q_j, \quad (4)$$

where the bar over the variables denotes values at the operating point and

$$a_{1,j} = \frac{D_{g,j} + \bar{P}_{l,j} D_{l,j}/(4\pi^2 \bar{f}_j)}{J_j}, \qquad a_{2,j} = \frac{1}{4\pi^2 \bar{f}_j J_j},$$

$$a_{3,j} = \frac{1}{\tau_{g,j}}.$$

B. WPP modelling

The response times of the VSCs in WPPs are much faster than the time constants expected in the dynamics of the AC areas given by (1) and (2). Hence, for control design purposes, WPPs can be modelled as power sources delivering into the DC grid a power

$$P_{w,j} = N_j \frac{\rho A_j}{2} C_P(\Omega_j, W_j, \theta_j) W_j^3, \quad j = 1, \dots, m,$$

where the WPPs are represented as aggregated models, and N_j is the number of wind turbines in the farm, A_j is the rotor area and ρ is the air density. The power coefficient C_P is a function of the pitch angle θ_j, the wind speed W_j, and the shaft speed Ω_j, which governs the energy captured by the wind rotor.

C. MT-HVDC grid modelling

The DC grid is described as a resistive electrical network, inductances and capacitances in cables are neglected as their dynamics are faster than those analyzed here. As a result, Station j is assumed delivering to the DC grid a power given by

$$P_{\mathrm{dc},j} = V_{\mathrm{dc},j} \sum_{k=1}^{n+m} \frac{V_{\mathrm{dc},j} - V_{\mathrm{dc},k}}{R_{jk}}, \quad (5)$$

where R_{jk} is the resistance between Stations j and k, and $V_{\mathrm{dc},j}$ is the DC voltage at the node j. If no direct electrical connection between the Stations j and k exists, R_{jk} is assumed infinite.

Linearizing (5) and defining $v_j = V_{\mathrm{dc},j} - \bar{V}_{\mathrm{dc},j}$, with $\bar{V}_{\mathrm{dc},j}$ the DC voltage at the operating point, the small-signal version of (5) results

$$u_j = \frac{\bar{P}_{\mathrm{dc},j}}{\bar{V}_{\mathrm{dc},j}} v_j + \bar{V}_{\mathrm{dc},j} \sum_{k=1}^{n+m} \frac{v_j - v_k}{R_{jk}}. \quad (6)$$

III. Control Strategy for Frequency Support

In this section, we propose a distributed control strategy to coordinate the power contributions of the WPPs in order to provide fast frequency compensation in the AC areas. The proposed control strategy consists of the following parts.

- Local power controls implemented at each station, basically an automatic generator control (AGC) in the AC areas and power generation control in the WPPs.
- A DC voltage control to ensure a proper power transmission under normal operation (droop control).
- A distributed control based on limited communication links aimed to restore or at least reduce the frequency deviation in all the AC areas using the power reserves in the WPPs.

Each part is explained in the next three subsections and a discussion about the coordination of all controls is presented in Section III-D.

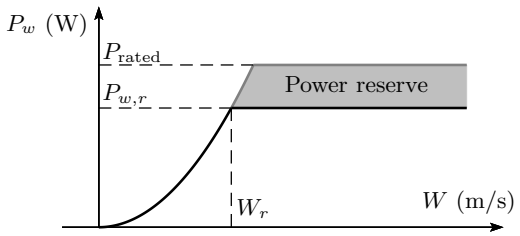

Figure 2. De-loading power control strategy in the WPPs

A. Local power control

1) WPP local control: The WPPs are assumed controlled using a de-loading strategy tracking a power reference according to the curve in Figure 2 [21]. Once the wind speed W reaches the value W_r, the power is maintained at a value $P_{w,r}$ lower than the rated value P_{rated} in order to have some power reserve for providing fast frequency support. Based on the assumption in Section II-B, this yields $P_{r,j+n} = P_{w,j} = P_{w,r,j}$.

2) Local frequency control at AC areas: Each AC area is equipped with a frequency control in order to ensure a long-term balance between generation and consumption at local level. This control acts as the well-known AGC imposing a power reference

$$q_j = -K_{fp,j} y_j - K_{Pi,j} \int x_j \, \mathrm{d}t, \tag{7}$$

where $K_{fp,j} = \bar{P}_{g,j}/\sigma_j \bar{f}_j$ [8] and $K_{Pi,j}$ a parameter to be designed [22]. The control law (7) aims to stop the frequency drop without power contributions from the multi-terminal grid. The last term in (7) ensures that the power demanded by the AC area to the MT-HVDC grid returns slowly to zero after the power imbalance. On one hand, this allow restoring the power reserves in the WPPs to the initial values. On the other hand, this ensures that the frequency can be restored locally, in case of lack of wind power reserves or fails in communication links.

The parameter $K_{Pi,j}$ is usually a small value and can be set according to the acceptable time for restoring the wind power reserve without affecting the capability of the whole system to provide frequency support.

B. Voltage control

In a MT-HVDC grid, the power transmission is ensured by regulating the DC voltage. Although there exist several control schemes, droop control is commonly used due to its high reliability. In normal operation, the stations on the AC areas are responsible for the DC voltage regulation of the entire MT-HVDC grid. The DC voltage droop control is basically a decentralized proportional law defined as

$$u_{V,j} = -K_{Vp,j} v_j, \quad j = 1, \ldots, n. \tag{8}$$

where $K_{Vp,j} = \bar{P}_{g,j}/V_{\text{nom}}$ and V_{nom} is the nominal DC voltage. Notice that the voltage droop control is implemented only in the AC stations.

C. MT-HVDC control for frequency support

The local controls are complemented with a communication-based scheme in order to coordinate the power contribution of the WPPs and thus to provide fast frequency support in the AC areas. For this purpose, let $\mathcal{C}_j$ be the set of communication links carrying frequency measures of other stations to the j-th station (e.g. $\mathcal{C}_j = \{i, k, h\}$ denotes that Station j receives frequency measures from Station i, k, and h), then the following control law is implemented in each AC area

$$u_{f,j} = \sum_{k \in \mathcal{C}_j} \alpha \int (y_j - y_k) \, \mathrm{d}t + \beta \, (y_j - y_k) \tag{9}$$

and the following one in each WPP

$$u_{w,j} = \begin{cases} u_{\min,j}, & \hat{u}_{w,j} < u_{\min,j}, \\ \hat{u}_{w,j}, & u_{\min,j} \le \hat{u}_{w,j} < u_{\max,j}, \\ u_{\max,j}, & \hat{u}_{w,j} \ge u_{\max,j}, \end{cases} \tag{10}$$

where

$$\hat{u}_{w,j} = \sum_{k \in \mathcal{C}_j} \alpha \int y_k \, \mathrm{d}t + \beta \, y_k,$$

$u_{\min,j}$ and $u_{\max,j}$ denote the minimum and maximum power reserve values, respectively. Expressions (9) and (10) are the set-points sent to the lower level controls in AC area and WPP stations. Notice that every station might not have full information regarding the status of the remaining stations. This covers for instance the circumstance in which fiber-optic links included in the DC cables are used to transmit the station status.

To sum up, combining (8)-(10) the coordinated control strategy for frequency support consists in

$$\begin{aligned} u_j &= u_{f,j} + u_{V,j}, && \text{for } j = 1, \ldots, n \quad \text{(AC areas)}, \\ u_{j+n} &= u_{w,j}, && \text{for } j = 1, \ldots, m \quad \text{(WPPs)}. \end{aligned}$$

In order to find the closed-loop system and determine the parameters α and β in the control laws (9) and (10), consider the following vectors

$$\begin{aligned} &\mathbf{y} = [y_1, \ldots, y_n]^T, && \mathbf{u} = [u_1, \ldots, u_{n+m}]^T, \\ &\mathbf{v} = [v_1, \ldots, v_{n+m}]^T, \end{aligned}$$

the Laplacian matrix $\mathbf{L}$ of dimension $n \times n$ corresponding to the communication graph among the different stations with elements

$$[\mathbf{L}]_{ji} = \begin{cases} -1 & \text{for } i \in \mathcal{C}_j, \\ -\sum_{k \in \mathcal{C}_j} [\mathbf{L}]_{jk} & \text{for } j = i, \end{cases}$$

the matrix $\mathbf{Q}$ of dimensions $m \times n$ with elements

$$[\mathbf{Q}]_{ji} = \begin{cases} 1 & \text{for } i \in \mathcal{C}_{j+m}, \\ 0 & \text{otherwise}, \end{cases}$$

and the diagonal matrix $\mathbf{H}_l$ of dimensions $m \times m$ and elements

$$[\mathbf{H}_l]_{jj} = \begin{cases} 1 & \text{if } u_{w,j} = \hat{u}_{w,j}, \\ 0 & \text{otherwise}, \end{cases}$$

where l enumerates the particular saturation configuration [23].

With this definitions, the control laws (9) and (10) result in

$$\mathbf{u}_a = \underbrace{\alpha \int \mathbf{L}\mathbf{y}\,\mathrm{d}t + \beta \mathbf{L}\mathbf{y}}_{\mathbf{u}_f} \underbrace{-\hat{\mathbf{K}}_{Vp}\mathbf{v}}_{\mathbf{u}_V},$$

$$\mathbf{u}_w = \mathbf{H}_l \left(\alpha \int \mathbf{Q}\mathbf{y}\,\mathrm{d}t + \beta \mathbf{Q}\mathbf{y} \right) + \bar{\mathbf{H}}_l \mathbf{u}_{\mathrm{sat}},$$

with $\bar{\mathbf{H}}_l + \mathbf{H}_l = \mathbf{I}_m$ (identity matrix), $\hat{\mathbf{K}}_{Vp} = \begin{bmatrix}\mathbf{K}_{Vp} & \mathbf{0}_{n\times m}\end{bmatrix}$, $\mathbf{K}_{Vp} = \mathrm{diag}(K_{Vp,1}, \ldots, K_{Vp,n})$, and $\mathbf{u}_{\mathrm{sat}}$ denotes the lower or upper saturation values.

The DC voltage equation (6) can be expressed as

$$\begin{bmatrix} \mathbf{u}_f - \hat{\mathbf{K}}_{Vp}\mathbf{v} \\ \mathbf{u}_w \end{bmatrix} = \left(\bar{\mathbf{P}}_{\mathrm{dc}} \bar{\mathbf{V}}_{\mathrm{dc}}^{-1} + \bar{\mathbf{V}}_{\mathrm{dc}} \mathbf{G} \right) \mathbf{v}$$

where $\bar{\mathbf{P}}_{\mathrm{dc}} = \mathrm{diag}(\bar{P}_{\mathrm{dc},1}, \ldots, \bar{P}_{\mathrm{dc},n+m})$, $\bar{\mathbf{V}}_{\mathrm{dc}} = \mathrm{diag}(\bar{V}_{\mathrm{dc},1}, \ldots, \bar{V}_{\mathrm{dc},n+m})$ and $\mathbf{G}$ the admittance matrix. Therefore,

$$\mathbf{v} = \left(\bar{\mathbf{P}}_{\mathrm{dc}} \bar{\mathbf{V}}_{\mathrm{dc}}^{-1} + \bar{\mathbf{V}}_{\mathrm{dc}} G + \begin{bmatrix} \hat{\mathbf{K}}_{Vp} \\ \mathbf{0} \end{bmatrix} \right)^{+} \begin{bmatrix} \mathbf{u}_f \\ \mathbf{u}_w \end{bmatrix} = \\ = \begin{bmatrix} \mathbf{T}_{11} & \mathbf{T}_{12} \\ \mathbf{T}_{21} & \mathbf{T}_{22} \end{bmatrix} \begin{bmatrix} \mathbf{u}_f \\ \mathbf{u}_w \end{bmatrix}.$$

where the superscript $(+)$ denotes the Moore-Penrose pseudo-inverse matrix. Thus, the power extracted by the AC areas from the MT-HVDC grid, including the effects of the droop control, results

$$\mathbf{u}_a = (\mathbf{I} - \mathbf{K}_{Vp}\mathbf{T}_{11})\mathbf{u}_f - \mathbf{K}_{Vp}\mathbf{T}_{12}\mathbf{u}_w.$$

Substituting these expressions of u_j in (3) and (4), the closed-loop system in matrix form is given by

$$\frac{\mathrm{d}\boldsymbol{\theta}}{\mathrm{d}t} = \mathbf{A}_{cl,l}\boldsymbol{\theta} - \mathbf{B}_{cl,l}\mathbf{d}, \tag{11}$$

where $\boldsymbol{\theta}^T = \begin{bmatrix}\mathbf{y}^T & \mathbf{x}^T & \boldsymbol{\varphi}^T & \boldsymbol{\mu}^T\end{bmatrix}$, $\boldsymbol{\varphi} = \int \mathbf{u}\,\mathrm{d}t$, $\boldsymbol{\mu} = \int \mathbf{y}\,\mathrm{d}t$,

$$\mathbf{A}_{cl,l} = \begin{bmatrix} -\mathbf{A}_1 - \beta\mathbf{A}_2\mathbf{F}_l & \mathbf{A}_2 & \mathbf{0} & -\alpha\mathbf{A}_2\mathbf{F}_l \\ -\mathbf{A}_3\mathbf{K}_{fp} & -\mathbf{A}_3 & \mathbf{A}_3 & \mathbf{0} \\ \beta\mathbf{F}_l & \mathbf{0} & \mathbf{0} & \alpha\mathbf{F}_l \\ \mathbf{I} & \mathbf{0} & \mathbf{0} & \mathbf{0} \end{bmatrix}$$

$$\mathbf{B}_{cl,l} = \begin{bmatrix}\mathbf{A}_2 & \mathbf{0} & \mathbf{0} & \mathbf{0}\end{bmatrix}^T,$$

$$\mathbf{A}_k = \mathrm{diag}(a_{k,1}, \cdots, a_{k,n}), \quad k = 1, 2, 3$$

$$\mathbf{F}_l = ((\mathbf{I} - \mathbf{K}_{Vp}\mathbf{T}_{11})\mathbf{L} - \mathbf{H}_l\mathbf{K}_{Vp}\mathbf{T}_{12}\mathbf{Q}).$$

Tuning of the control law (9) requires the selection of two scalar parameters α and β. The simplest method is set $\alpha = \beta$ and find the value that produces a suitable closed-loop pole locations for (11). For the system under study, this method might achieve a reasonable frequency regulation.

Alternatively, it can be used optimal control concepts to find two independent values of α and β that stabilize (11) and ensure certain performance criterion [24]. More concretely, the closed-loop matrix can be expressed as

$$\mathbf{A}_{cl} = \begin{bmatrix} -\mathbf{A}_1 & \mathbf{A}_2 & \mathbf{0} & \mathbf{0} \\ -\mathbf{A}_3\mathbf{K}_{fp} & -\mathbf{A}_3 & \mathbf{A}_3 & \mathbf{0} \\ \mathbf{0} & \mathbf{0} & \mathbf{0} & \mathbf{0} \\ \mathbf{I} & \mathbf{0} & \mathbf{0} & \mathbf{0} \end{bmatrix} + \begin{bmatrix} -\mathbf{A}_2 \\ \mathbf{0} \\ \mathbf{I} \\ \mathbf{0} \end{bmatrix} \underbrace{\begin{bmatrix}\alpha\mathbf{I} & \beta\mathbf{I}\end{bmatrix}}_{\mathbf{K}} \begin{bmatrix} \mathbf{0} & \mathbf{0} & \mathbf{0} & \mathbf{F}_l \\ \mathbf{F}_l & \mathbf{0} & \mathbf{0} & \mathbf{0} \end{bmatrix}$$

and defining $\mathbf{z}^T = \begin{bmatrix}\mathbf{W}_e\boldsymbol{\mu}^T & \mathbf{W}_u\mathbf{u}_a\end{bmatrix}^T$ as a performance output, then the tuning of the coordinated control gains results in computing a static-output feedback gain $\mathbf{K}$ such us

$$\|\mathbf{z}\|_2 < \gamma \|\mathbf{d}\|_2, \tag{12}$$

where $\gamma > 0$ is a real scalar, and $\mathbf{W}_e$ and $\mathbf{W}_u$ are weighting transfer functions. The weight $\mathbf{W}_e$ penalizes the frequency deviations and $\mathbf{W}_u$ the control actions. Thus, the optimization based on criterion (12) seeks to find a trade-off between a good frequency regulation and reasonable control inputs. This can be solved for instance with algorithms like those given in [25].

D. Coordination of each control level

The different control levels working together ensure the power transmission and the provision of fast frequency support.

- The droop law (8) regulates the voltage at all terminals and thus ensuring the proper power transmission in normal operation.
- The local power control law (7) in the AC areas forces the long-term local power balance between generation and consumption.
- The aim of the high-level distributed control laws (9) and (10) is to coordinate the contribution of the WPPs and the power extraction from the MT-HVDC grid to provide a fast frequency restoration when a power imbalance in the AC areas arises.

The last term in (7) forces a local power balance in long-term without contributions from the MT-HVDC grid. Thus, the power reserves in the WPPs are restored to the initial values. The control (9) seeks to share the power reserve among the AC area to minimize the frequency deviations. The control (10) seeks to increase the power contribution from the WPPs in order to minimize the frequency error y_j and make the frequencies in all AC areas close to the nominal values.

Comparing with the control scheme in [20], the control strategy introduced in this section includes the local power control (7) and the droop law (8). The former is needed to restore the wind power reserves and is not considered in [20]. The drop control replaces the master-slave scheme in [20], this improves reliability but also participates in the coordinated response aimed at regulating the frequency and must be considered in the control tuning. Furthermore, the new scheme uses less information as can be observed in (9). In this case, the controls implemented in the AC areas need some partial information about the frequency in other areas but no information about the WPP contributions.

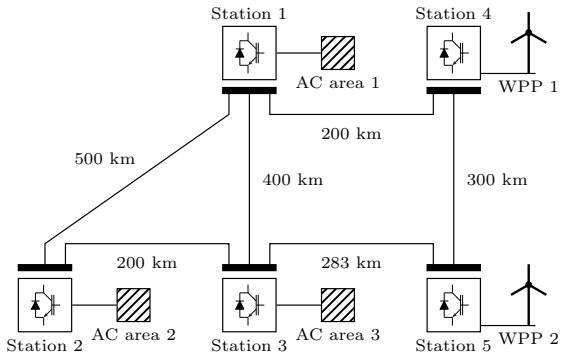

Figure 3. Power system analyzed in the case study

Table I
PARAMETERS CORRESPONDING TO POWER SYSTEM UNDER STUDY

AC area j	1	2	3
J_j (kgm^2)	64845.60	145902.50	64845.60
$D_{g,j}$ (kWs^2)	60.79	81.06	60.79
$D_{l,j}$ (s)	0.08	0.10	0.08
$\tau_{g,j}$ (s)	6.00	8.00	6.00
$\bar{P}_{g,j}$ (MW)	799.30	1207.50	801.30
$K_{fp,j}$ (MW/Hz)	799.30	1106.80	801.30
$K_{fi,j}$ (1/s)	0.30	0.30	0.30
σ_j (s)	0.02	0.0218	0.02
$\bar{f}_j$ (Hz)	50.00	50.00	50.00
Line resistances	$R_{12} = 9.5\,\Omega$	$R_{13} = 7.6\,\Omega$	$R_{14} = 3.8\,\Omega$
	$R_{23} = 3.8\,\Omega$	$R_{25} = 5.4\,\Omega$	$R_{45} = 5.7\,\Omega$

IV. CASE STUDY

The proposed frequency control strategy was evaluated by simulation in a commonly used multi-terminal network [26] with small changes for frequency control studies. In particular, the case study corresponds to a MT-HVDC grid with three AC areas and two WPPs ($n = 3$ and $m = 2$) as illustrated in Figure 3. Table I lists the parameters of each AC area and the MT-HVDC network. WPP 1 and WPP 2 correspond to wind farms with eighty 5 MW-turbines and seventy 5 MW-turbines, respectively, modelled as aggregated turbines using a two-mass model. The wind turbines corresponds to the NREL benchmark turbine proposed in [27]. AC areas 1, 2 and 3 are assumed generating 799.30 MW, 1207.50 MW and 801.30 MW, respectively. Simulations were performed with Simulink and Simscape.

The DC voltage in the MT-HVDC grid is controlled using a droop strategy with constants $K_{Vp,j} = \bar{P}_{g,j}/V_{\text{nom}}$ at the AC stations ($j = 1, 2, 3$), where the nominal DC voltage is $V_{\text{nom}} = 400$ kV. The local power controllers were designed according to (7), the resulting values are given in Table I.

It is assumed that communications among stations are implemented via the fiber-optic links included in the DC cables. Therefore, in this case, the communication scheme is given by

$$\mathcal{C}_1 = \{2, 3\}, \quad \mathcal{C}_2 = \{1, 3\}, \quad \mathcal{C}_3 = \{1, 2\},$$
$$\mathcal{C}_4 = \{1, 3\}, \quad \mathcal{C}_5 = \{1, 3\}.$$

It can be observed that there is no direct communication-link between the WPPs and AC area 2. For the design procedure in Section III-C, this implies that

$$\mathbf{L} = \begin{bmatrix} 2 & -1 & -1 \\ -1 & 2 & -1 \\ -1 & -1 & 2 \end{bmatrix}, \qquad \mathbf{Q} = \begin{bmatrix} 1 & 0 & 1 \\ 1 & 0 & 1 \end{bmatrix}.$$

Notice that in this case, the frequency deviations in Station 2 are not directly available for the controls in WPPs. The parameters for the distributed control strategy were tuned as indicated in Section III-C, in which the weighting functions were set as

$$\mathbf{W}_e(s) = \mathbf{I}, \qquad \mathbf{W}_u(s) = 0.05\,\frac{0.1s + 1}{0.001s + 1}\,\mathbf{I}.$$

The weight W_e penalizes the frequency deviations and W_u the fast changes in the DC powers (control actions). With this setup, the optimization problem in Section III-C produces the following parameters for the distributed frequency control

$$\alpha = 176.03 \text{ MW}, \qquad \beta = 70.28 \text{ MWs}.$$

Three scenarios are considered to evaluate the proposed control strategy. The first analyzes the case when the WPPs have direct communication links with the AC areas in which increases in power demand cause frequency falls. The second consider the case when the WPPs do not have direct information about the frequency disturbances. Lastly, the behavior under some communication failures is analyzed.

A. Scenario 1: changes in $P_{l,1}$ and $P_{l,3}$

This scenario analyzes the system response when the power demands in AC areas 1 and 3 change. The wind speed was set at 13 m/s in both WPPs, therefore both wind farms are working above rated wind speed (region 3). The total wind power delivered to the grid is 675 MW ($\bar{P}_{w,1} = 360$ MW and $\bar{P}_{w,2} = 315$ MW), reserving a 10% of the power capacity to provide frequency support. The initial power demands are $P_{l,1} = 980$ MW, $P_{l,2} = 1515$ MW and $P_{l,3} = 980$ MW. At $t = t_1$, the power demand in AC area 3 rises in 59.95 MW (7.5% of $P_{l,1}$) and at $t = t_2$ the power demand in AC area 1 increases in 59.95 MW. Figure 4a shows the frequency evolution when only the local control is applied. Notice that the NADIR frequency for both areas is below the admissible value 49.80 Hz given in the grid codes.

The system response when the proposed control scheme provides frequency support is shown in Figure 5. The top plot corresponds to the frequency at each AC area and the lower one to the incremental power values injected and extracted by the VSCs at each terminal of the MT-HVDC grid. For $t_1 \leq t \leq t_2$, the coordinated control establishes an equal power contributions from both WPPs. It can be observed that only small contributions is required from the other AC areas as the power reserves in the WPPs are enough to balance this rise in the power demand. The small frequency changes in the undisturbed stations are caused mainly by the change in the power flow and the droop control. A subsequent increase in the power demand $P_{l,1}$ occurs at $t = t_2$. Under this circumstance, the WPPs are not capable of bringing the frequencies back

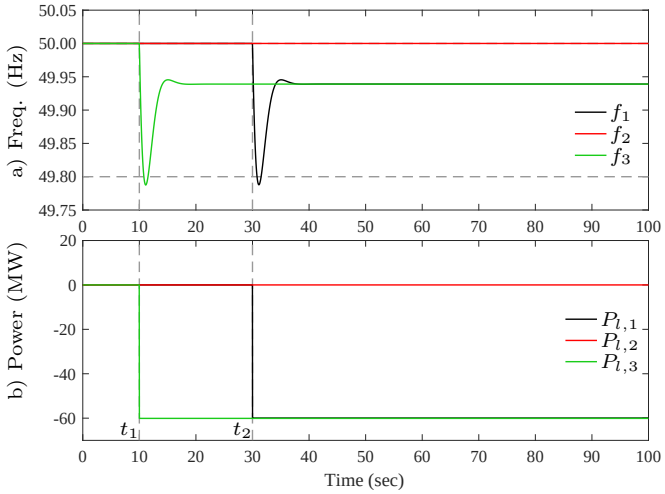

Figure 4. Scenario 1: a) Frequencies and b) power demands (disturbances) without the proposed frequency control

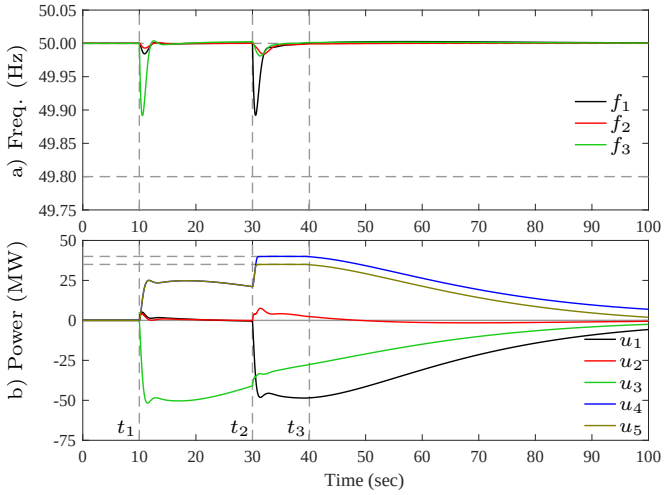

Figure 5. Scenario 1: a) Frequencies and b) DC powers for the closed-loop system with the proposed frequency control scheme

to the nominal values in all AC areas and the other areas must contribute to reduce the frequency falls. The local power controllers increase the power generation in all AC areas. At $t = t_3$, the increase in AC area generation allows the WPPs to enter linear zone and the coordinated control is now able to drive the frequency deviations in all AC areas to zero. The slow increase of the generation in the AC areas, as a consequence of the local power control, allows the WPPs to recover the power reserves. Figure 6 shows the powers extracted by each AC area decomposed into the droop control part $u_{v,j}$ (expression (8)) and the frequency control part $u_{f,j}$ (expression (9)).

B. Scenario 2: changes in $P_{l,2}$ and $P_{l,3}$

The second scenario analyzes a similar case but with an increase in the power demand in Station 2 instead of in Station 1. This is a more demanding scenario as the WPPs do not have direct communication-link with Station 2. Figure 7 displays the system response when the coordinated control is

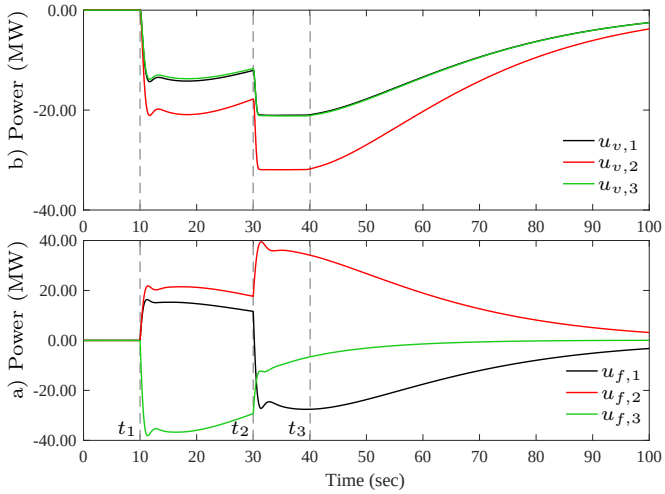

Figure 6. Scenario 1: DC powers a) from droop control ($u_{v,j}$) and b) from frequency control ($u_{f,j}$) for the closed-loop system with the proposed frequency control scheme

not applied. The starting conditions are the same to those in the previous scenario. In this case, the power demand increases in 84.52 MW (7% of $P_{l,2}$) at $t = t_2$. In this case, the NADIR frequency is lower than 49.80 Hz, although a less significant fall is observed in f_3.

The closed-loop response with the proposed coordinated control can be observed in Figure 8. In this case, the frequency drop after the increase in the power demand at $t = t_2$ is more significant. Clearly, the lack of direct communication links between the WPPs and Station 2 results in a more marked initial contribution from Station 1. However, the coordinated control scheme is able to rapidly deduce the disturbance from the frequency deviations in the other AC areas and find a consensus to reduce the frequency drop in Station 2. It can also be observed a larger time interval in which the WPPs are delivering the maximum power. This is a consequence of the more significant increase in the power demand, compared with the previous case. This circumstance also allows a better observation of the contributions of the all AC areas to find a common frequency closer to the nominal value as a result of the consensus imposed by the proposed control strategy forces. The corresponding parts of the DC powers extracted by each AC area can be seen in Figure 9.

C. Scenario 3: communication failures

In the last scenario, the power demand changes discussed in Scenario 2 were repeated but now considering two communication failures.

Figure 10 displays the frequencies and the DC powers when the power demands change as in Figure 7b. In this case, it is assumed that Stations 4 and 5 (WPP1 and WPP2) do not receive the frequency measure from Station 1 and 3, respectively. This situation results in a change in the matrix $\mathbf{Q}$ as follows

$$\mathbf{Q} = \begin{bmatrix} 1 & 0 & 0 \\ 0 & 0 & 1 \end{bmatrix}.$$

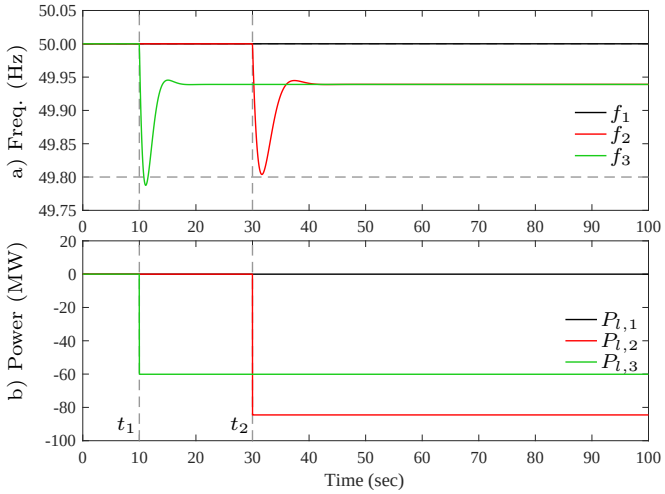

Figure 7. Scenario 2: a) Frequencies and b) power demands (disturbances) without the proposed frequency control

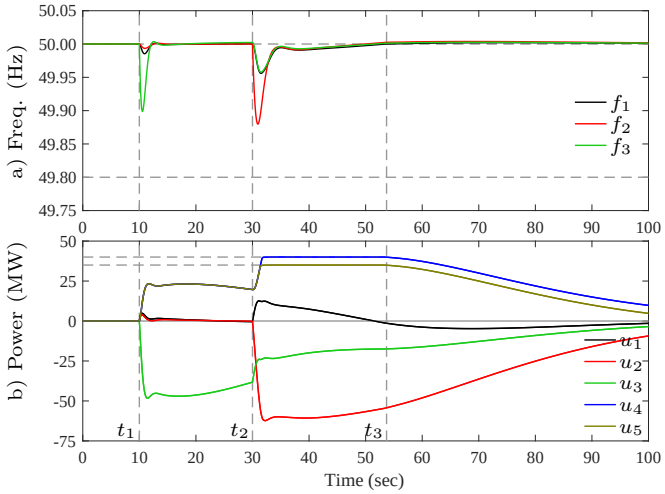

Figure 8. Scenario 2: a) Frequencies and b) DC powers for the closed-loop system with the proposed frequency control scheme

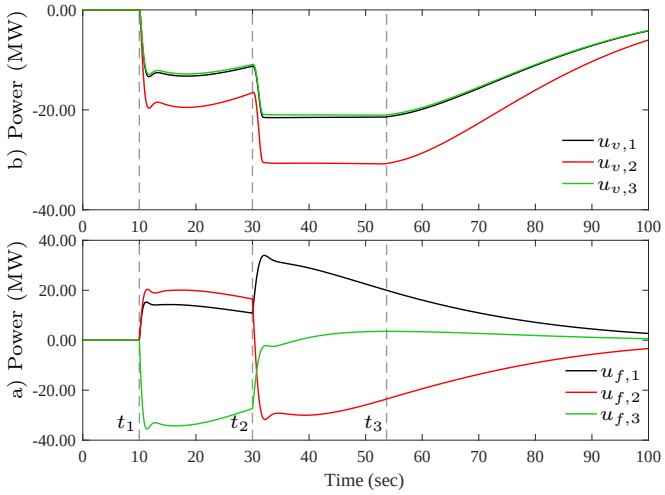

Figure 9. Scenario 2: DC powers a) from droop control ($u_{v,j}$) and b) from frequency control ($u_{f,j}$) for the closed-loop system with the proposed frequency control scheme

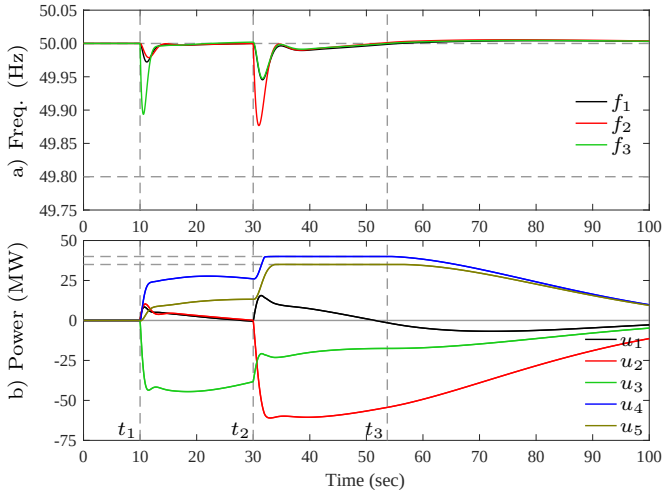

Figure 10. Scenario 3: a) Frequencies and b) DC powers for the closed-loop system with the proposed frequency control scheme considering the loss of communication between Stations 1 and 5 and Stations 3 and 4, respectively

It can be observed in Figure 10 that there is no a significant change in the frequency regulation compared to Figure 8. However, the contributions of the WPP and even the AC areas have changed. This is a consequence of the less information that each WPP has, resulting in a not so well coordinated actions from the WPPs that makes the frequency regulation a little slower.

On the other hand, if it is assumed that the communication link between Stations 1 and 3 is lost, the matrix $\mathbf{Q}$ remains unchanged but the Laplacian matrix changes to

$$\mathbf{L} = \begin{bmatrix} 2 & -1 & 0 \\ -1 & 2 & -1 \\ 0 & -1 & 2 \end{bmatrix}.$$

The system response can be seen in Figure 11 under the same power demand profiles in Figure 7b. In this case, the changes in the frequency regulation are less significant. The small changes can be explained as a consequence that Station 1 detects the change in $P_{l,2}$ indirectly through the DC network instead of a faster communication channel.

These two simulations show that even under communication failures, the proposed control is still capable of properly regulating the frequency. Furthermore, the new control strategy was able to restore the frequency in all the cases.

V. Conclusions

The proposed control seeks to coordinate the power contribution of WPPs to MT-HVDC networks in order to mitigate the frequency fluctuations in AC areas. This article extends a previous results on distributed control of MT-HVDC grids by considering the limitation on communication-links and the use of local power controls to restore the power reserves in WPPs. Simulations show that even without a direct communication link with the disturbed AC area, the proposed control is capable of reducing the frequency drops. Moreover, the control scheme is also able to limit the frequency deviations in situations with power imbalances in the AC areas higher than the total power reserves available in the WPPs.

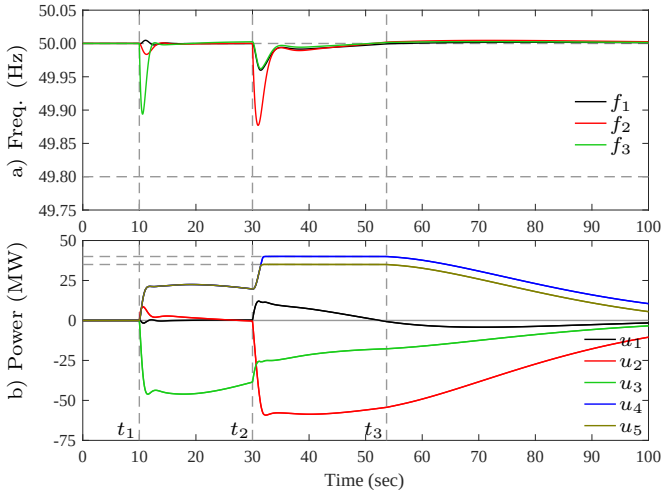

Figure 11. Scenario 3: a) Frequencies and b) DC powers for the closed-loop system with the proposed frequency control scheme considering the loss of communication link between Stations 1 and 3

APPENDIX

List of Symbols

f_j	Electrical frequency
$P_{l,j}$	Power demand in AC area j
$P_{\mathrm{dc},j}$	DC power at Station j
Pr	AC set-point power at Station j
y_j	Incremental frequency
d_j	Incremental power demand in AC area j
u_j	Incremental DC power at Station j
$u_{v,j}$	Incremental DC power due to droop control
$u_{f,j}$	Incremental DC power due to frequency control
$u_{w,j}$	Incremental DC power injected by WPP

REFERENCES

[1] A. Arapogianni, J. Moccia, and J. Wilkes, "The European offshore wind industry - key trends and statistics 2012," European Wind Energy Association, Tech. Rep., 2013.

[2] S. Gordon, "SuperGrid to the rescue," *IET Power Eng.*, vol. 20, no. 5, pp. 30–33, 2006.

[3] D. Van Hertem and M. Ghandhari, "Multi-terminal VSC HVDC for the European supergrid: Obstacles," *Renewable Sustainable Energy Rev.*, vol. 14, pp. 3156–3163, 2010.

[4] J. Liang, T. Jing, O. Gomis-Bellmunt, J. Ekanayake, and N. Jenkins, "Operation and Control of Multiterminal HVDC Transmission for Offshore Wind Farms," *IEEE Trans. Power Del.*, vol. 26, no. 4, pp. 2596–2604, 2011.

[5] F. D. Bianchi, J. L. Domínguez-García, and O. Gomis-Bellmunt, "Control of multi-terminal HVDC networks towards wind power integration: A review," *Renewable Sustainable Energy Rev.*, vol. 55, pp. 1055–1068, mar 2016.

[6] P. M. Anderson and A. A. Fouad, *Power System Control and Stability*, 2nd ed. New York, USA: John Wiley & Sons Inc, 2002.

[7] ENTSO-E, "Future system inertia," Apr. 2014.

[8] P. Kundur, *Power System Stability and Control*. New York, USA: McGraw-Hill, 1994.

[9] F. Díaz-González, M. Hau, A. Sumper, and O. Gomis-Bellmunt, "Participation of wind power plants in system frequency control: Review of grid code requirements and control methods," *Renewable Sustainable Energy Rev.*, vol. 34, pp. 551–564, 2014.

[10] R. G. de Almeida and J. A. Pecas Lopes, "Participation of doubly fed induction wind generators in system frequency regulation," *IEEE Trans. Power Syst.*, vol. 22, no. 3, pp. 944–950, 2007.

[11] N. Ullah, T. Thiringer, and D. Karlsson, "Temporary primary frequency control support by variable speed wind turbines – potential and applications," *IEEE Trans. Power Syst.*, vol. 23, no. 2, pp. 601–612, 2008.

[12] J. Aho, A. Buckspan, and J. H. Laks, "A tutorial of wind turbine control for supporting grid frequency through active power control," in *Proc. Amer. Control Conf*, 2012, pp. 3120–3131.

[13] J. Dai, Y. Phulpin, A. Sarlette, and D. Ernst, "Coordinated primary frequency control among non-synchronous systems connected by a multi-terminal high-voltage direct current grid," *IET Gener. Transm. Distrib.*, vol. 6, no. 2, p. 99, 2012.

[14] A. Sarlette, J. Dai, Y. Phulpin, and D. Ernst, "Cooperative frequency control with a multi-terminal high-voltage DC network," *Automatica*, vol. 48, no. 12, pp. 3128–3134, Dec. 2012.

[15] N. Chaudhuri, R. Majumder, and B. Chaudhuri, "System frequency support through multi-terminal DC (MTDC) grids," *IEEE Trans. Power Syst.*, vol. 28, no. 1, pp. 347–356, 2013.

[16] M. Andreasson, R. Wiget, D. V. Dimarogonas, K. H. Johansson, and G. Andersson, "Distributed primary frequency control through multi-terminal HVDC transmission systems," in *Proc. Amer. Control Conf*, Chicago, USA, 2015.

[17] A. M. Bucurenciu, "Primary frequency response by MTDC offshore grids," Master's thesis, Delft University of Technology, 2012.

[18] B. Silva, C. Moreira, L. Seca, Y. Phulpin, and J. Peças-Lopez, "Provision of inertial and primary frequency control services using offshore multi-terminal HVDC networks," *IEEE Trans. Sustain. Energy*, vol. 3, no. 4, pp. 800–808, 2012.

[19] I. Martinez Sanz, B. Chaudhuri, and G. Strbac, "Inertial response from offshore wind farms connected through DC grids," *IEEE Trans. Power Syst.*, vol. 30, no. 3, pp. 1518–1527, 2015.

[20] F. D. Bianchi and J. L. Domínguez-García, "Coordinated Frequency Control Using MT-HVDC Grids With Wind Power Plants," *IEEE Trans. Sustain. Energy*, vol. 7, no. 1, pp. 213–220, jan 2016.

[21] P. Sorensen, A. D. Hansen, F. Iov, F. Blaabjerg, and M. H. Donovan, "Wind farm models and control strategies," RISO, Tech. Rep. Riso-R-1464, 2005.

[22] P. M. Namara, R. Meere, T. O'Donnell, and S. McLoone, "Control strategies for automatic generation control over MTDC grids," *Control Eng. Pract.*, vol. 54, pp. 129–139, sep 2016.

[23] F. Bullo, J. Cortes, and S. Martinez, *Distributed control of robotic networks*. Princeton, USA: Princeton University Press, 2009.

[24] R. S. Sánchez Peña and M. Sznaier, *Robust Systems Theory and Applications*. New York, USA: Wiley-Interscience, 1998.

[25] P. Gahinet and P. Apkarian, "Automated tuning of gain-scheduled control systems," in *Proc. 52nd Conf. Decision Control*, 2013, pp. 2740–2745.

[26] Cigré, "Guide for the development of models for HVDC converters in a HVDC grid," 2015.

[27] J. Jonkman, S. Butterfield, W. Musial, and G. Scott, "Definition of a 5-MW reference wind turbine for offshore system development," NREL, Golden, Colorado, USA, Tech. Rep. NREL/TP-500-38060, 2009.